Electronic Supplementary Material (ESI) for Molecular Systems Design & Engineering.

SUPPLEMENTARY INFORMATION

Nanothin Film Conductivity Measurements Reveals Interfacial Influence on Ion Transport in Polymer Electrolytes

Ban Xuan Dong[1], *Peter W. Bennington*[1], *Yu Kambe*[1,2], *Daniel Sharon*[1], *Moshe Dolejsi*[1], *Veronica Burnett*[1], *Joseph Strzalka*[3], *Paul F. Nealey*[1,2] *and Shrayesh N. Patel*[1,4,*]

[1]*Institute for Molecular Engineering, University of Chicago, Chicago, Illinois 60637, USA*

[2]*Materials Science Division, Argonne National Laboratory, Lemont, Illinois 60439, USA*

[3]*X-ray Science Division, Argonne National Laboratory, Argonne, Illinois 60439, United States*

[4]*Chemical Sciences and Engineering Division, Argonne National Laboratory, Argonne, Illinois 60439, United States*

*Correspondence to shrayesh@uchicago.edu

1. Fabricating procedures of IDEs

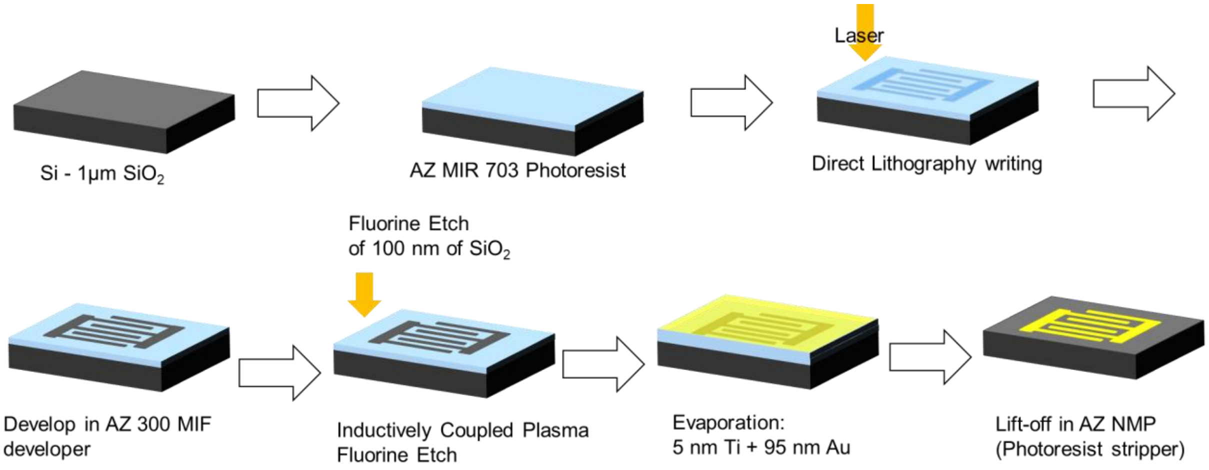

Figure S1: Fabricating procedures of IDE devices. The IDEs were fabricated at PNF cleanroom, University of Chicago

The fabricating procedures of IDE devices is shown in Figure S1. Silicon wafers with a 1000 nm thick, thermally grown oxide (Silicon Wafer Inc.) were baked for 30 min at 90°C before subjected to 25 s of O_2 plasma cleaning to maximize the density of -OH groups on top of SiO_2 surface. The wafers were then coated with bis(trimethylsilyl)amine (HMDS) using vapor prime method prior to coating with ca. 1µm layer of the positive photoresist AZ MIR 703. In the next step, the wafers were soft-bake at 90°C for 1 min before being exposed to a 405 nm laser at 90 mJ/cm^2 dosage using a Heidelberg MLA150 Direct Write Lithographer with pre-defined IDE patterns. The exposed wafers were developed in an AZ300 MIF developer with agitation for ca. 1 min before rising in DI water for ~ 1 min and subjected to 25 s of O_2 plasma for descumming the surface. Inductively Coupled Plasma Fluoride Etch was utilized to etch down 100 nm of SiO_2. The wafers were subjected to 25 s of O_2 plasma for descumming the residual etching materials prior to deposition of 5 nm Ti/95 nm Au metals to the wafers. The purpose of etching is to fabricate IDEs with “sunken” electrodes. After metal deposition, the photoresist layer was lift-off by extended soak in hot NMP (4+ hours at 80°C) followed by sonication in fresh NMP and IPA. In the final step, the wafers were rinsed in DI water for ~ 1 min, dry and subjected to 25 s of O_2 plasma again for final cleaning of the surface.

2. GIWAXS measurement and analysis

GIWAXS measurements were performed at beamline 8-ID-E of the Advanced Photon Source, Argonne National Laboratory with 10.86 keV (λ = 0.11416 nm) synchrotron radiation. Samples were measured inside a low vacuum chamber (10^{-3} mbar) to minimize concerns about radiation damages, samples' moisture uptake as well as prevent extraneous scattering from ambient air. The measurement time was chosen to be 4 second per frame. For each sample, 3 data sets were taken from 3 adjacent spots on the sample and then averaged in order to enhance the signal-to-noise ratio. In our work, the samples were tilted at an angle of incidence of 0.14° with respect to the incoming beam, which is above the estimated critical angle of sample (ca. 0.13°) but below the critical angle of the Si substrates (ca. 0.17°) in order to probe the whole film thickness and further enhance signal-to-noise ratio. The scattering signal was recorded with a Pilatus 1MF pixel array detector (pixel size = 172 µm) positioned 228 mm from the sample. Each data set was stored as a 981x1043 32-bit tiff image with 20-bit dynamic range. The Pilatus detector has rows of inactive pixels at the border between detector modules. In order to fill these gaps, after each measurement the detector was moved to a new vertical direction and the measurement on each spot was repeated, then the gaps were filled by combining the data from two detector positions. The signals were reshaped and output as intensity maps in q_z vs q_r (= $\sqrt{q_x^2 + q_y^2}$) space. We also performed corrections for detector nonuniformity, detection efficiency, the polarization effect and solid-angle variation for each image. All the GIWAXS data processing and extraction were executed using the GIXSGUI package for MATLAB.[1]

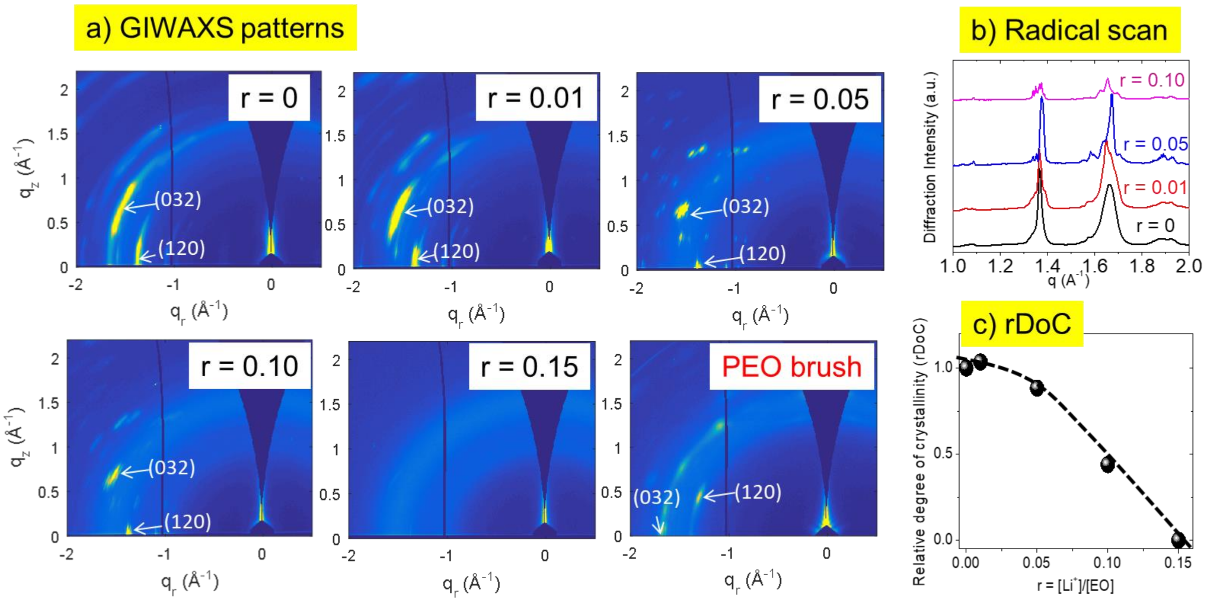

Figure S2: (a) Geometrically corrected GIWAXS diffraction pattern of PEO brush and PEO-LiTFSI thin film blends at different salt concentrations. (b) 1-D intensity distribution after integrating the 2-D data along the azimuthal direction (radical scan). Curves are offset for clarity (c) Estimated relative degree of crystallinity of PEO at different LiTFSI concentration

Grazing incidence wide-angle X-ray scattering (GIWAXS) was carried out to investigate the crystallite structure of PEO upon introducing LiTFSI. Geometrically corrected room temperature GIWAXS patterns of PEO-LiTFSI thin film fabricated on top of the PEO brush at different concentration *r* along with the GIWAXS pattern of the PEO brush are shown in Figure S2a. To identify PEO crystallite orientation, we focus on the position of the two diffraction peaks (032) near q = 1.7 Å^{-1} and (120) near q = 1.4 Å^{-1} (indicated by the arrows in Figure S2a) as done in prior studies.[2,3] Except for the highest Li salt containing sample r = 0.15 where no discernable diffraction peaks were observed, the diffraction patterns of all PEO-LiTFSI samples appear qualitatively similar. The GIWAXS patterns of all four samples r = 0 (neat PEO), 0.01, 0.05 and 0.1 show the maximum of the (120) diffraction peak near the horizon at q_z =0, but the maximum for the (032) peak occurs off the horizon at $q_z \approx 0.6 Å^{-1}$. According to the simulation performed by Asada and co-workers,[2] this observation suggest that in the PEO-LiTFSI thin films, the polymer crystallites adopt the "edge-on" orientation in which the PEO chains are oriented parallel to the substrate. Moreover, with increasing LiTFSI content, both the (032) and (120) peak shapes become sharper and the diffraction intensity becomes weaker, indicating that adding LiTFSI induces highly oriented crystals but reduces overall degree of crystallinity of PEO samples. The PEO structure becomes completely amorphous at the highest blending concentration $r = 0.15$. In stark contrast to the PEO-LiTFSI films, the GIWAXS pattern of the PEO brush exhibits the (032) peak at the horizon instead, suggesting bias toward "flat-on" orientation in which the PEO chains prefer to lie perpendicular to the underlying substrate.[2] Here, it is important to note that in our GIWAXS measurements, we chose the incidence angle $\alpha = 0.14°$ which is above the critical angle of the samples in order to probe the structure of the whole films. Interestingly, for all PEO-LiTFSI samples we do not observe the diffraction features of the underlying PEO brush despite the fact that the PEO-LiTFSI samples were fabricated on top of it. This observation suggests that the PEO brush re-crystallizes and intermixes with the PEO-LiTFSI layer during the fabrication process.

In order to compare the relative degree of crystallinity (rDoC) at different concentration r in a more quantitative manner, we first perform the radial line cuts as a function of q, followed by appropriate background subtraction (Figure S2b). To permit an accurate comparison of rDoC, all PEO-LiTFSI samples were prepared at approximately the same total thickness $h \sim 25$ nm. Additionally, X-ray exposure time and beam foot-print size were made the same for all samples.[4] We also assume that the structure factor is similar across the samples, which is reasonable given their similar GIWAXS patterns. Following previous studies on PEO films,[5,6] we calculate rDoC by integrating the diffraction intensity of the radial line cut and then normalizing the integrated intensity by the estimated volume fraction of PEO in the PEO-LiTFSI mixtures. The calculated rDoC as a function of LiTFSI concentration *r* is plotted in Figure S2c. As seen in Figure S2c, the rDoC of PEO-LiTFSI thin films is found to monotonically decrease with increasing *r* and the structure becomes completely amorphous at $r = 0.15$. This trend is similar to various previous bulk studies on PEO-Li salt mixtures which also suggested the reduction of overall PEO degree of crystallinity upon blending with Li salts.[6–8]

3. Ionic conductivity during the heating and cooling cycles

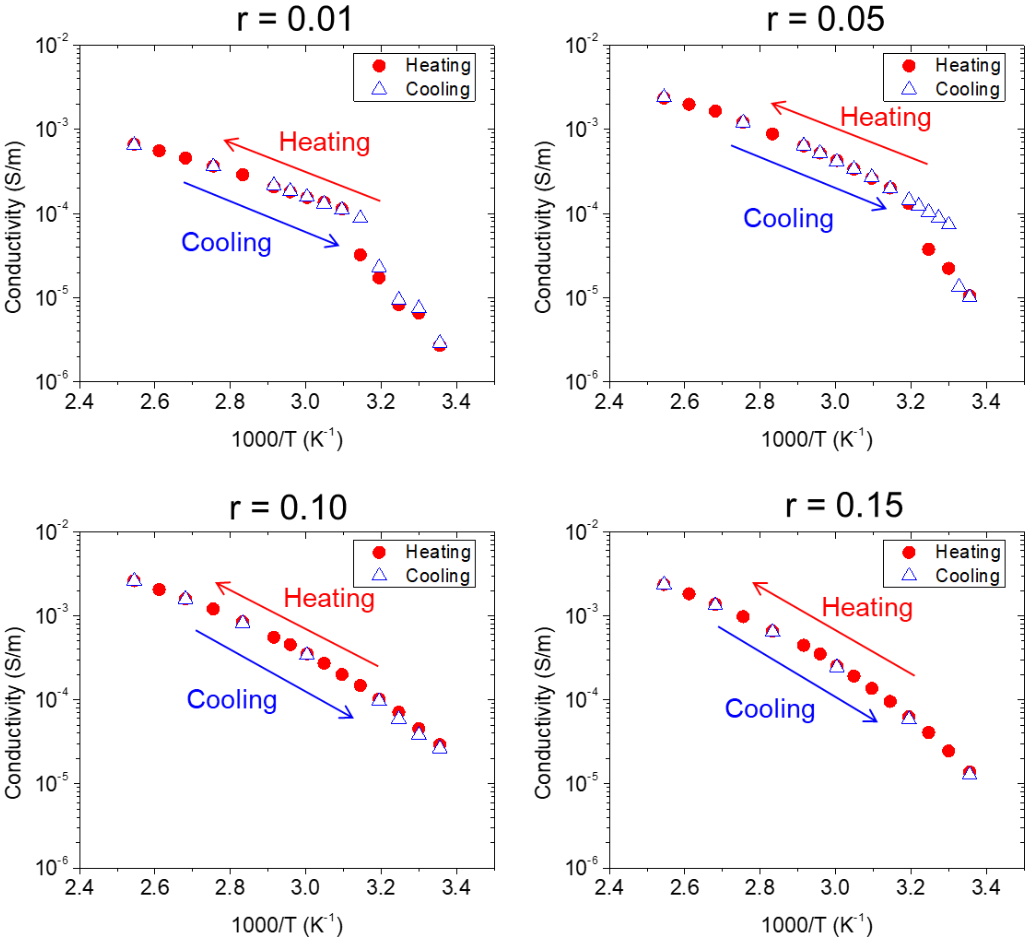

Figure S3: Ionic conductivity of 25 nm PEO-LiTFSI samples at different salt concentrations during the first heating and then cooling cycles.

4. Extracted parameters from impedance measurements shown in Figure 2b

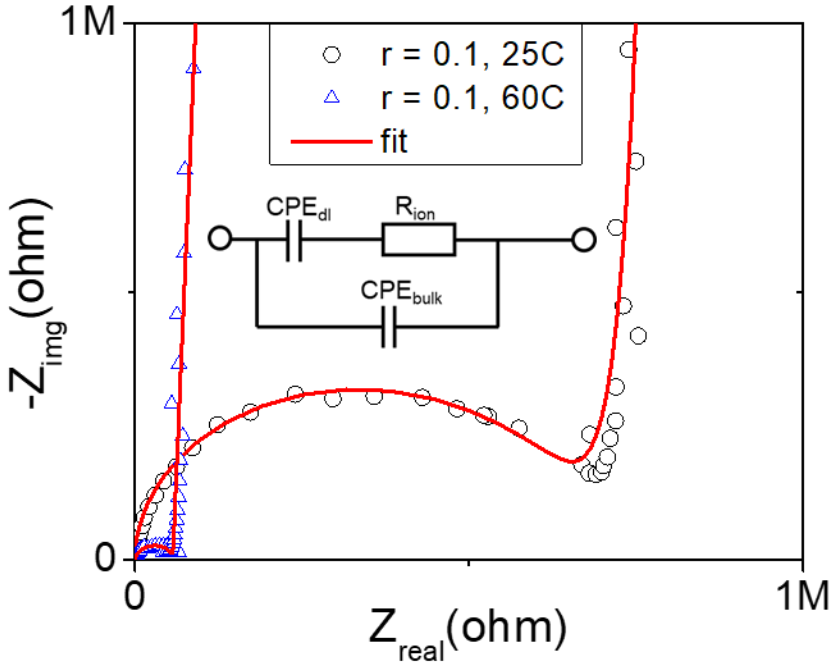

Figure S4: Exemplary Nyquist Impedance plots of 25 nm PEO-LiTFSI thin film at 25C and 60C. The same data is shown in the main manuscript Figure 2b. Solid lines represent the fit to impedance data using the simplified equivalent circuit shown in the inset of the figure.

Table S1: Extracted fitted parameters of the impedance data shown in Figure S4

	r = 0.1, 25C	***r = 0.1, 60C***
R_{ion}	7.3×10^{5} Ω	5.8×10^{3} Ω
Q_{bulk}	1.31×10^{-10} Fs^{a-1}	1.47×10^{-10} Fs^{a-1}
a_{bulk}	0.95	0.87
Q_{dl}	7.3×10^{-9} Fs^{a-1}	7.8×10^{-9} Fs^{a-1}
a_{dl}	0.99	0.98

5. Extracted parameters from VTF fit

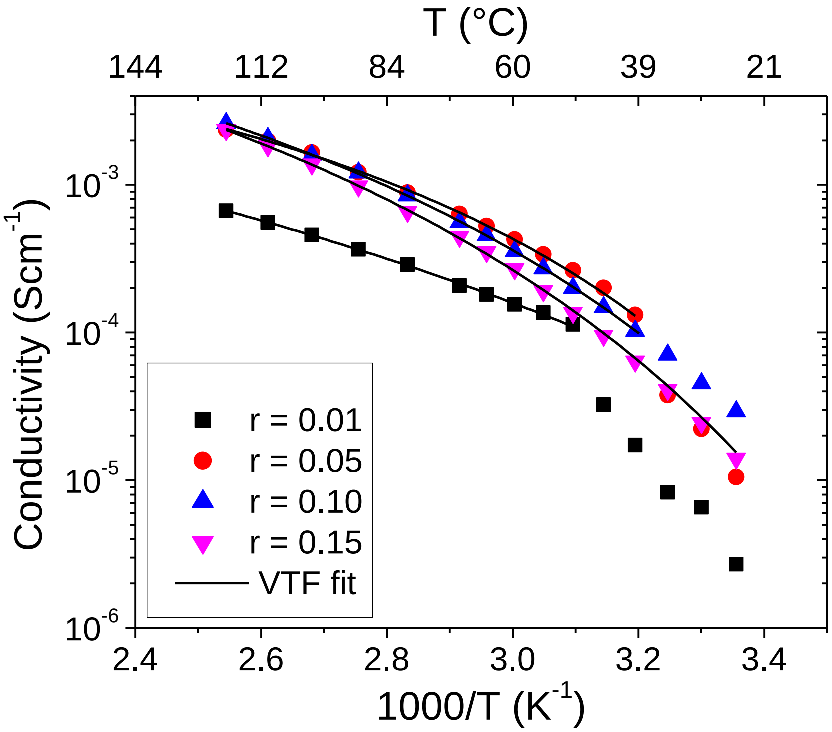

Figure S5: Temperature dependence of ionic conductivity at different salt concentrations. The solid black lines represent the fit to Vogel-Tamman-Fulcher (VTF) model at each concentration r. Thickness h of all sample is ca. 25 nm. The same data is shown in the main manuscript Figure 2c

Table S2: Extracted fitted VTF parameters of the conductivity data shown in Figure S5

r	**B (K)**	**σ_0(S/cm)**	**T_0(K)**
0.01	800	2.7E-2	178
0.05	425	3.7E-2	237
0.10	650	0.12	220
0.15	731	0.16	218

6. Thickness dependence conductivity of r = 0.01 and r = 0.15 samples at all temperature

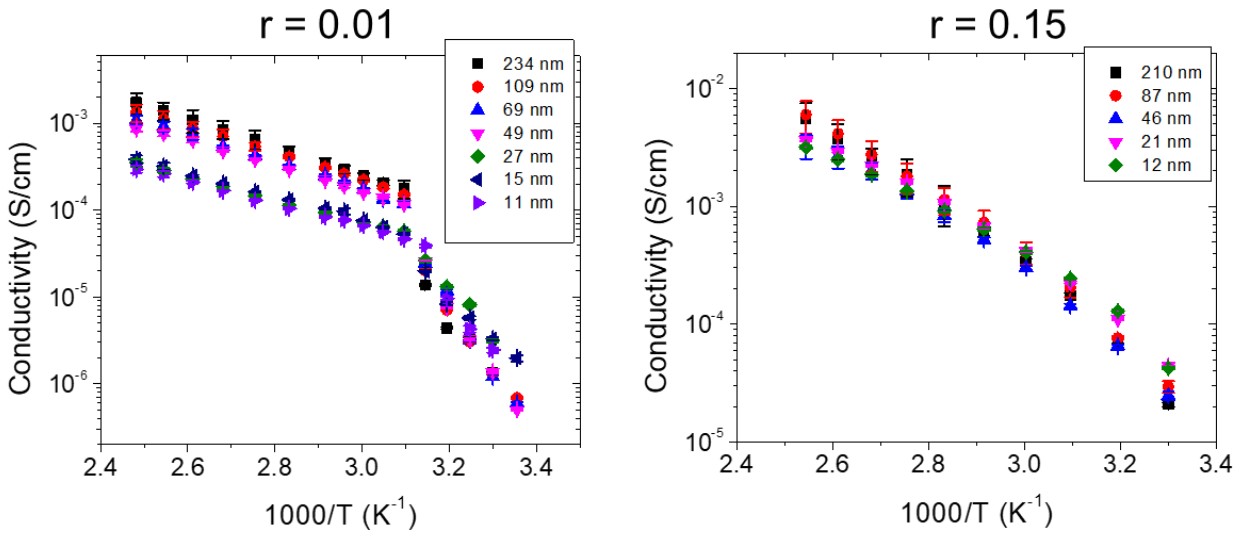

Figure S6: Thickness dependence conductivity of r = 0.01 and r = 0.15 samples. The data was taken during the first heating cycles.

7. VTF fit for r = 0.15 at different film thicknesses

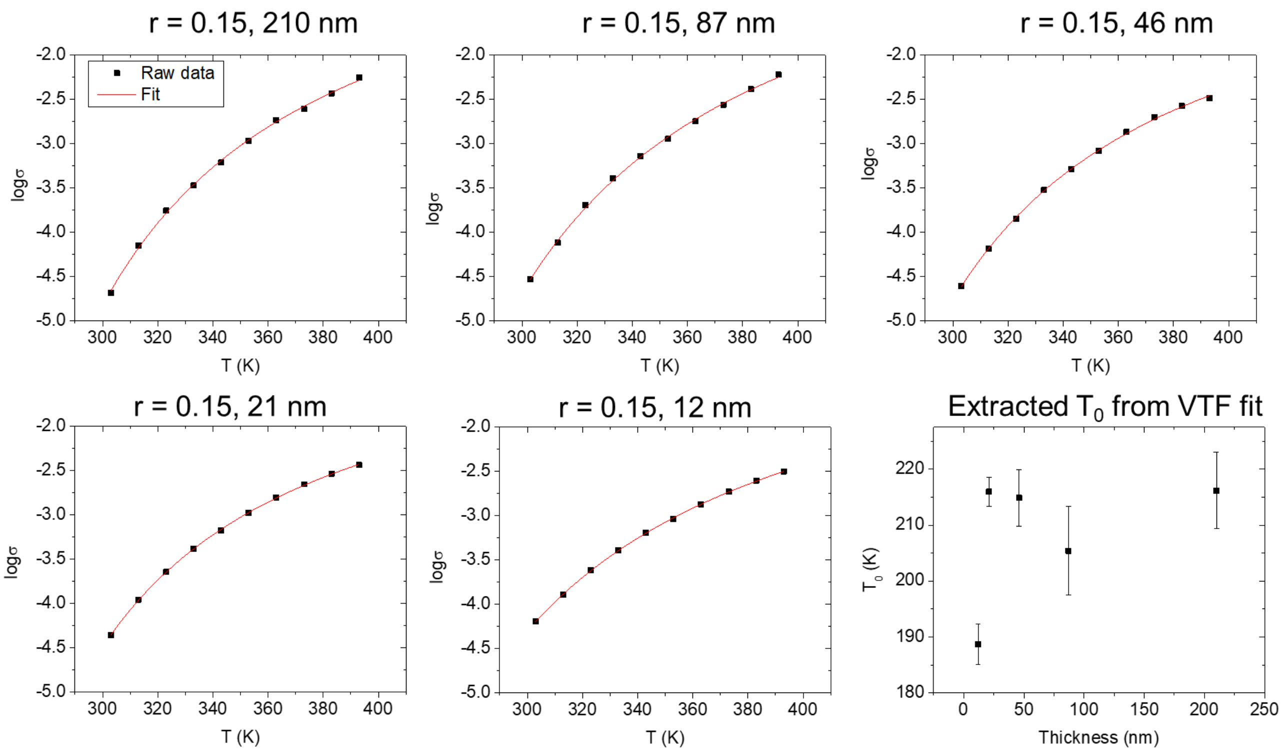

Figure S7: VTF fit for r = 0.15 at different film thicknesses and the extracted fitting parameters for T_0

8. Thickness dependent conductivity fit

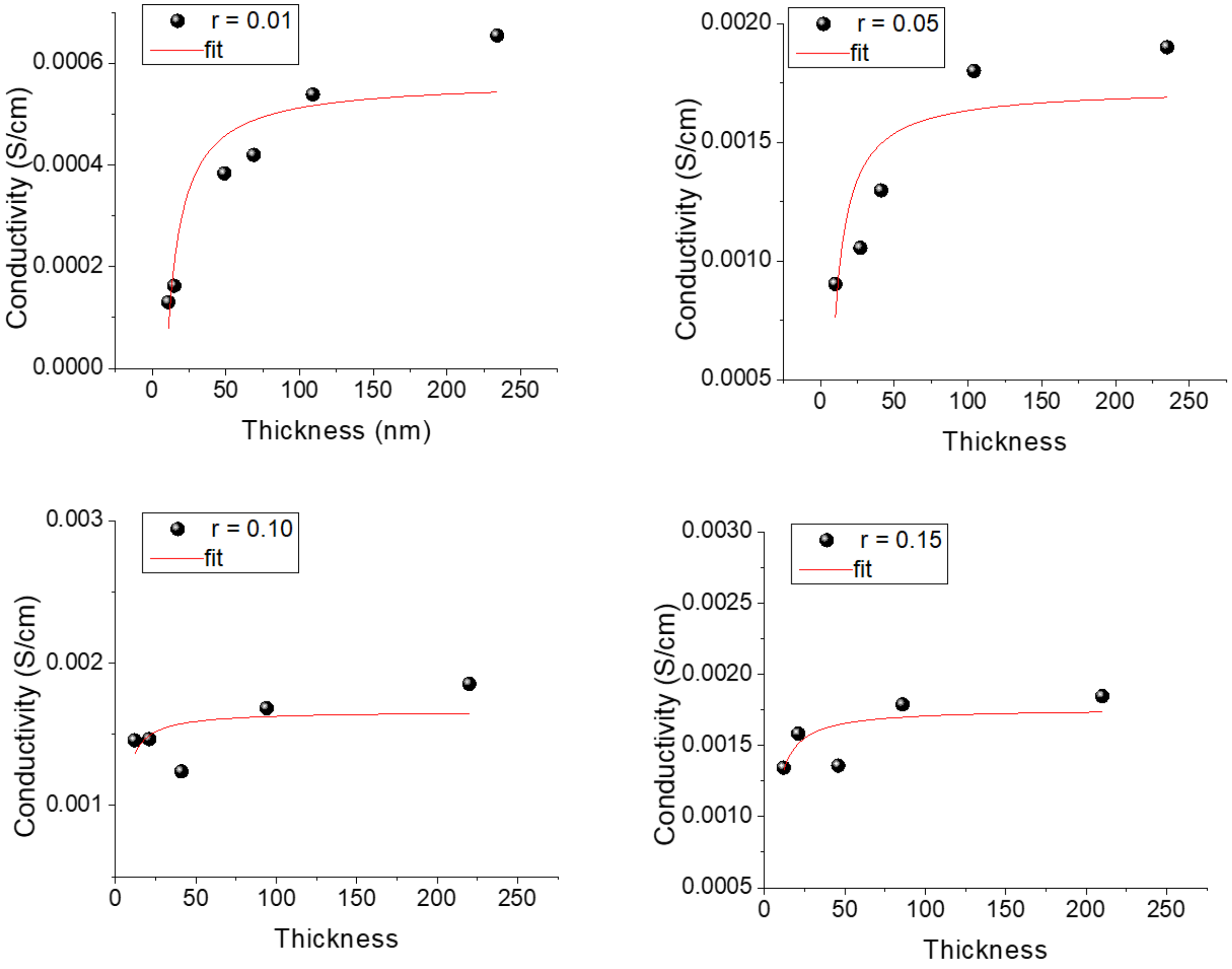

Figure S8: Fit of thickness dependent conductivity at different LiTFSI concentration

9. Estimation of SEO chain density

This section provides a rough estimation of chain density in lamella forming SEO block copolymer. We utilize the established chain stretching length d as a function of chain length N in strong segregation limit introduced by Singh et al.[9] $d = 0.41 \times N^{0.68}$. The chain density is then calculated using the following equation:

$$\rho_{chain,SEO} = \frac{d \times \rho_{SEO} \times N_A}{M_{SEO}}$$

Here ρ_{SEO} = 1.105 g/cm^3 is SEO density. Using the above equation, we can calculate SEO chain density as a function of MW, the result of which is plotted in the following:

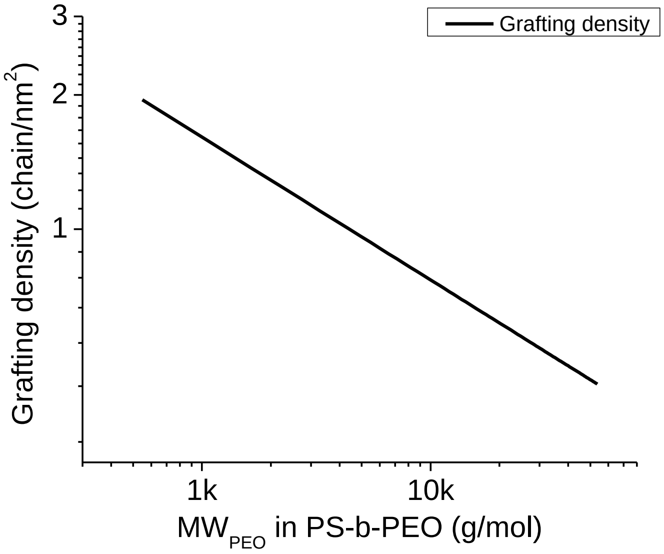

Figure S9: The chain density at PS/PEO interface in SEO as a function of MW of the PEO block

10. REFERENCE

1 Z. Jiang, *J. Appl. Crystallogr.*, 2015, **48**, 917–926.

2 M. Asada, N. Jiang, L. Sendogdular, J. Sokolov, M. K. Endoh, T. Koga, M. Fukuto, L. Yang, B. Akgun, M. Dimitriou and S. Satija, *Soft Matter*, 2014, **10**, 6392–6403.

3 M. Asada, N. Jiang, L. Sendogdular, P. Gin, Y. Wang, M. K. Endoh, T. Koga, M. Fukuto, D. Schultz, M. Lee, X. Li, J. Wang, M. Kikuchi and A. Takahara, *Macromolecules*, 2012, **45**, 7098–7106.

4 B. X. Dong, A. Li, J. Strzalka, G. E. Stein and P. F. Green, *J. Polym. Sci. Part B Polym.*

Phys., 2017, **55**, 39–48.

5 D. T. W. Toolan, A. Isakova, R. Hodgkinson, N. Reeves-Mclaren, O. S. Hammond, K. J. Edler, W. H. Briscoe, T. Arnold, T. Gough, P. D. Topham and J. R. Howse, *Macromolecules*, 2016, **49**, 4579–4586.

6 S. Cheng, D. M. Smith and C. Y. Li, *Macromolecules*, 2014, **47**, 3978–3986.

7 S. Lascaud, M. Perrier, A. Vallee, S. Besner, J. Prud'homme and M. Armand, *Macromolecules*, 1994, **27**, 7469–7477.

8 S. K. Fullerton-Shirey and J. K. Maranas, *Macromolecules*, 2009, **42**, 2142–2156.

9 M. Singh, O. Odusanya, G. M. Wilmes, H. B. Eitouni, E. D. Gomez, A. J. Patel, V. L. Chen, M. J. Park, P. Fragouli, H. Iatrou, N. Hadjichristidis, D. Cookson and N. P. Balsara, *Macromolecules*, 2007, **40**, 4578–4585.